Mössbauer spectrometry of Fe(Cu)MB-type nanocrystalline alloys: I. The fitting model for the Mössbauer spectra

1997 J. Phys.: Condens. Matter 9 2303

(http://iopscience.iop.org/0953-8984/9/10/017)

J. Phys.: Condens. Matter **9** (1997) 2303–2319. Printed in the UK PII: S0953-8984(97)78324-3

Mössbauer spectrometry of Fe(Cu)MB-type nanocrystalline alloys: I. The fitting model for the Mössbauer spectra

Marcel Miglierini† and Jean-Marc Greneche

Laboratoire de Physique de l'Etat Condensé, URA CNRS 807, Université du Maine, F72017 Le Mans Cédex, France

Received 2 October 1996, in final form 9 December 1996

Abstract. A fitting model based on the use of two independent blocks resulting from distributions of a hyperfine field and of one sextet of lorentzian lines is discussed for Mössbauer spectra recorded for Fe(Cu)MB nanocrystalline alloys. One distributed subspectrum is ascribed to the amorphous residual matrix, while the other independent block, from the hyperfine-field distribution, is attributed to Fe atoms located in the so-called interface zone. This region comprises atoms of nanocrystalline-grain surfaces and also atoms originating from the amorphous precursor, in close contact with the nanocrystalline grains. A sextet of lorentzian lines is attributed to the crystalline grains that have emerged from the amorphous alloy, which are unambiguously identified as α-Fe phase. The distribution with low hyperfine fields can be eventually analysed in terms of two components accounting for the coexistence of electric and magnetic hyperfine interactions. In such an analysis, distributions of both quadrupolar splittings and hyperfine magnetic fields are employed. Examples of the present fitting model are provided for Mössbauer spectra of FeCuMB (M = Zr, Ti, and NbCr) nanocrystalline alloys in the first stage of crystallization. The spectra have been recorded under various experimental conditions comprising low (77 K) and high (373 K) temperatures as well as an external magnetic field. More detailed discussion about the consequences of this novel fitting procedure with respect to the topography of hyperfine interactions within Fe-based nanocrystalline alloys is reported in part II, the following paper.

1. Introduction

Nanocrystalline ferromagnets offer new opportunities for technological applications, because of their excellent soft magnetic properties. The nanocrystalline state which is obtained by a partial devitrification of the amorphous state consists of ultra-fine crystalline grains embedded in the remaining amorphous matrix. The magnetic softening is essentially due to the nanoscale structure, i.e. the presence of small grains which induce the suppression of the local magneto-crystalline anisotropy by exchange interactions [1].

So we focused our attention on the understanding of the structural and magnetic properties of the intergranular zone, as well as its influence on the magnetic softening. For most nanocrystalline alloys, x-ray diffraction may yield an estimate of the average crystal size and the nature of the crystalline phase, whereas static magnetic data have to be carefully discussed because they result from both crystalline and non-crystalline phases. In contrast, ^{57}Fe Mössbauer spectrometry is an excellent tool for investigating these materials, because

† On leave from: Department of Nuclear Physics and Technology, Slovak Technical University, Ilkovičova 3, 812 19 Bratislava, Slovakia (e-mail: bruno@elf.stuba.sk). This is also the address for any correspondence.

0953-8984/97/102303+17$19.50

it permits one to elucidate the nature of both electric and magnetic hyperfine interactions of the different resonating iron nuclei and to probe their immediate surroundings [2].

So, we point out in the present paper first the role played by Mössbauer spectrometry in investigating iron-based amorphous and nanocrystalline alloys, with an overview of some fitting models generally used in recent studies, and then the lack of further interpretation of hyperfine data in conjunction with the structural behaviour of the material. We discuss also the ability of some alloys to exhibit experimental features providing us with accurate data relating to the intergranular phase: Fe(Cu)MB alloys seem more appropriate candidates than Fe(Cu)MBSi alloys, because the presence of Si within the crystalline phase induces a rather complex hyperfine structure, preventing one from finding a precise quantitative interpretation. In the last section, we introduce a novel fitting model which takes into account different structural positions of resonant atoms located in crystalline grains and the amorphous residual matrix. We discuss the model using Mössbauer spectra of several Fe(Cu)MB nanocrystalline alloys taken under different measuring conditions. The following paper is devoted to the application of the fitting procedure presented to the study of hyperfine interactions of $Fe_{87.5-x}Cu_xZr_{6.5}B_6$ ($x = 0, 1$) nanocrystalline alloys, to model the intergranular phase [3].

2. Mössbauer spectra analysis

2.1. Amorphous alloys

During the last two decades, Mössbauer spectrometry has played an essential role in the investigation of structural properties of amorphous materials [4, 5]. Indeed, both quadrupolar and magnetic Mössbauer spectra, which exhibit line broadening due to structural disorder, can be interpreted in terms of local disorder: in the magnetically ordered temperature range, the distributions of hyperfine fields can be correlated with the distribution of Fe coordination. The determination of the distribution of hyperfine fields, however, requires great care in the fitting procedure, because both the broadening and the overlapping of Mössbauer lines, as well as the magnetic texture, may be sources of possible misinterpretation [5–7]. Three main fitting procedures can be distinguished: (i) the most frequently used involves a distribution of hyperfine parameters without any *a priori* assumptions as to the shape; (ii) those for which an analytical form is assumed for the distribution; and (iii) those based on a description in terms of a superimposition of discrete fields in conjunction with a structural atomic model. Surveys of the different Mössbauer fitting methods can be found in two reviews [5, 8].

2.2. Fitting procedures for the Mössbauer spectra of Fe(Cu)MBSi nanocrystalline alloys

Mössbauer spectra of Fe-based nanocrystalline materials prepared by thermal annealing of amorphous alloys show well resolved and sharp absorption dips which are superimposed on broad line features. The sharp lines indicate the presence of crystallites which have emerged from the originally amorphous precursor (broad lines) in the course of the heat treatment. In the case of Fe(Cu)MBSi alloys, they are attributed to bcc-FeSi ultra-fine crystalline grains with Fe located at different structural positions. Consequently, most Mössbauer studies gave only reasonable estimates of the crystalline fraction and of the Si content within the crystalline phase. Nevertheless, one can find a variety of approaches used to derive the spectral parameters, and, hence, the hyperfine characteristics of both the crystalline components and the amorphous residual phases. A short overview of some fitting models used for Mössbauer spectra recorded for nanocrystalline alloys is presented below.

The simplest procedure uses pure lorentzian profiles to reconstruct the sharp lines of the crystalline structure, and one broadened sextet of lorentzian lines to fit the intergranular phase [9, 10]. Alternatively, the component attributed to the amorphous phase occurring in nanocrystalline samples is analysed using pseudo-lorentzian lines [11]. An attempt to account for the distribution of hyperfine fields is reported in [12] where the lineshape of the amorphous-phase component was treated using a Voigt profile. However, no other details are given regarding the hyperfine-field distribution in terms of the short-range-order arrangement of the amorphous residual matrix.

An original procedure for fitting the amorphous-phase subspectrum was presented by Pundt *et al* [13]. From the spectrum of the thermally treated samples, the broadened spectral component was evaluated using a data file which was obtained by measuring the Mössbauer spectrum of the as-quenched alloy, at room temperature. Only the relative area of this component was fitted. The crystalline component of the respective spectra was fitted by Zeeman-split patterns using five lorentzian sextets. Since one of them exhibited a rather large linewidth, it was assigned to a new 'emaciated' amorphous phase [13]. Thus, two different amorphous phases were considered for the annealed samples: one having the same hyperfine-field distribution as the as-quenched alloy; and a new 'emaciated' amorphous phase. The interest in such an approach lies in its introduction of different kinds of atomic disorder [13]. The only weak point is that there is no argument for assuming unchanged chemical and/or topological short-range order in the remaining amorphous part, which is described by a data set obtained from the corresponding as-quenched, i.e. non-thermally treated, alloy. In fact, one may expect some changes in the short-range order of the amorphous remainder, as a consequence of the partial devitrification induced in the course of the thermal treatment. That is why the description of the intergranular phase by means of a distribution of components seems to be more physically favourable [14–24].

The number of crystalline components in Fe-based Si-containing nanocrystalline alloys varies between four [9, 10, 12, 13], five [17], six [11] and seven [15, 16] sextets. Let us also mention that in recent studies of nanocrystalline materials, some authors have considered only distributions of hyperfine fields that are either gaussian [17] or double-gaussian asymmetrical functions [15]. Because chromium is known to lower the Curie temperature and to reduce the mean value of the hyperfine field, its addition to amorphous FeCuNbBSi alloys allows one to better separate the two components attributed to the nanocrystalline grains and to the amorphous matrix in the Mössbauer spectra obtained for $Fe_{66}Cr_8Cu_1Nb_3B_9Si_{13}$ nanocrystalline alloys [25]. Great attention was devoted to the fitting procedure which leads to an estimate of the crystalline fraction, and the Si content in the nanocrystalline grains is in nice agreement with those obtained from other techniques; the presence of a cusp in the temperature dependence of the hyperfine field of the nanocrystalline phase suggested the role of the intergranular phase, but the complexity of the Mössbauer spectra prevents further accurate interpretation [25, 26].

So, from this brief survey, it is obvious that making a proper choice of fitting procedure is not a trivial task. Each approach has its own advantages as well as shortcomings, and often compromise solutions must be looked for.

2.3. Fitting procedures for the Mössbauer spectra of Fe(Cu)MB nanocrystalline alloys

The first step of crystallization in Fe(Cu)MB alloys is characterized by the presence of only α-Fe grains [18–24]. Unlike in Si-containing materials, where the bcc-FeSi crystalline phase yields a complex Mössbauer spectrum with many components, the Mössbauer spectrum of an Fe(Cu)MB nanocrystal contains only one well resolved sextet of sharp lines corresponding to

bcc-Fe superimposed on a broad line feature due to the intergranular phase. The hyperfine parameters of bcc-Fe are well known, thus allowing us to concentrate on the remaining spectral components.

Double-peak behaviour of the hyperfine-field distribution was reported by Gorría *et al* [19] and Orúe *et al* [20] for $Fe_{86}Zr_7Cu_1B_6$ nanocrystalline alloys, using the modified and extended method of Billard and Chamberod. Navarro *et al* [21] have analysed room temperature Mössbauer spectra of $Fe_{88}Zr_7Cu_1B_4$ using the NORMOS program, and the distributions of hyperfine fields derived are attributed to the presence of two magnetically different regions. In our earlier work on a $Fe_{87.5-x}Zr_{6.5}Cu_xB_6$ system, we have employed the NORMOS program as well, and obtained a well separated bimodal profile $P(H)$ using a single block of hyperfine-field distribution [18]. Gómez-Polo *et al* [22] have used distributions of hyperfine fields to describe the residual amorphous matrix, a sextet characteristic of the precipitated α-Fe crystalline phase, and a quadrupolar doublet associated with a non-ferromagnetic Fe phase in $Fe_{87.2}Zr_{7.4}Cu_{1.1}B_{4.3}$ nanocrystalline alloy. No closer description and/or explanation of the fitting procedure is given in their paper, however.

The complex structure of the $P(H)$ distributions with two distinguished ranges of H-values which is presented in [18–22] suggests the presence of two magnetically as well as structurally distinct surroundings of the resonant atoms. The $P(H)$ contributions corresponding to higher values of hyperfine fields are ascribed to Fe_3B [19] or Fe–B [20] crystalline phases, but no experimental support for this assignment is provided from other techniques (e.g. x-ray diffraction). In fact, only reflections corresponding to the α-Fe crystalline phase and to the amorphous residual matrix are present in x-ray diffractograms of thermally treated $Fe_{86.5}Zr_{6.5}Cu_1B_6$ alloy up to the annealing temperature of 600 °C [3]. Beyond this temperature, a small amount of ZrO_2 crystalline phase appears; some borides are evident after annealing at 840 °C, which is already well above the temperature of the first crystallization step. They make up, however, less than 2% as estimated from the Mössbauer spectra. Our results are in agreement with the findings from the x-ray diffraction measurements, resistivity measurements, transmission electron microscopy, and magnetic measurements of other authors, performed upon the same [27] or very similar [28] alloys.

3. Experimental details

Amorphous $Fe_{86.5}Zr_{6.5}Cu_1B_6$, $Fe_{80}Ti_7Cu_1B_{12}$, and $Fe_{73.5}Nb_{4.5}Cr_5Cu_1B_{16}$ alloys have been prepared by a rapid solidification of the melt using the melt-spinning technique in the form of ribbons (width: 3–10 mm; thickness: 20–24 μm). Their amorphicity was checked by x-ray diffraction and by Mössbauer spectrometry. Thermal treatments were carried out in a protective atmosphere or in vacuum for one hour at temperatures of 600, 470, and 590 °C. We verified by x-ray diffraction that the nanocrystalline phase is due to bcc-Fe ultra-fine grains with sizes in the range 10–20 nm for low annealing temperatures. Mössbauer spectra were collected in transmission geometry by a conventional constant-acceleration spectrometer using a ^{57}Co(Rh) source of γ-radiation. The temperature of the measurement varied in the range 77 K to 373 K. The sheets of ribbons were located using either a bath cryostat or a cryofurnace, under a protective atmosphere or vacuum, respectively, to prevent any oxidation. Room temperature Mössbauer spectra were recorded after those at elevated temperatures to check the non-evolution of the nanocrystalline state. Small permanent magnets ($H_{ext} \approx 0.05$ T and 0.3 T) were applied to ensure parallel orientation of magnetic domains within the plane of the ribbon-shaped samples, i.e. perpendicular to the γ-beam, in order to reduce the number of fitting parameters.

The hyperfine parameters were refined using the NORMOS DIST [29] program as

described in the next section. For some spectra, a comparison was made with the MOSFIT program [30]: the discrepancy between the results was found to be lower than the experimental error. The proportions of iron crystalline and amorphous phases are taken to be proportional to their absorption areas, assuming the recoilless fractions to be identical for the two kinds of iron site. The isomer shift values are quoted relative to the spectrum for α-Fe at 300 K.

Moreover, the use of three-dimensional mapping of the distribution of hyperfine fields enables a better visualization of the evolution of the hyperfine interactions to be achieved [16, 18, 23, 24]; the temperature of the measurement [23], the annealing temperature [24], and the duration of the heat treatment [16] are the usual parameters used to establish the third dimension of 3-D $P(H)$ diagrams.

4. Description of the present fitting procedure

The high-field component of $P(H)$ is found positioned at around 30 T at room temperature whatever fitting procedure has been applied [18–22]. We can speculate that it is attributable to those Fe atoms which have mostly other Fe atoms as their nearest neighbours. Taking into account that only α-Fe crystalline grains are revealed in the Fe(Cu)MB-type nanocrystalline alloys, one can expect structurally different kinds of resonant Fe atom. A schematic representation is shown in the upper part of figure 1: one can distinguish: (i) atoms located in the bulk of α-Fe crystalline grains; (ii) Fe atoms which belong structurally to the nanocrystals but constitute the outer surfaces of grains; (iii) atoms situated in the nanocrystal-to-amorphous interface which originate from the amorphous precursor but are in close contact with nanocrystalline grains; and, finally, (iv) the disordered atomic arrangement within the amorphous residual matrix which is not in direct contact with nanocrystals. So, atoms (ii) and (iii) form an interfacial region.

From the structural point of view, Fe atoms (i) are perfectly ordered (bcc-type): they can be represented by a usual sextet of sharp lorentzian lines. Atoms (iii) and (iv) are randomly arranged, which means that a distribution of the respective hyperfine parameters should be employed to reconstruct their contribution to the overall Mössbauer spectrum. Due to the nanometric scale of the crystalline grains, Fe atoms (ii) located in the crystals' surfaces also play an important role, and their contribution, to some extent structural but mainly magnetic, cannot be neglected. Because the atoms (ii) are situated in the outer surfaces of nanocrystals and are in close contact with the intergranular phase, they might exhibit a certain degree of structural disorder. For that reason, a distribution of hyperfine parameters should also be expected.

As far as hyperfine interactions are concerned, it is not possible to distinguish unambiguously between the contributions of Fe atoms from group (ii) and from group (iii) to the total $P(H)$ curve. This is understandable because there exist certain areas inside the nanocrystalline alloy where the two kinds of atom face each other—that is why both might have the same or very close H-values. In other words, magnetic states of the neighbouring atoms transform continuously without any sudden modifications due to the penetration of the exchange interactions [31]. The range of this 'transition zone' depends on many parameters among which the size of the grains and their mutual separation are the most important [32]. Hyperfine interactions in nanocrystalline alloys are discussed in more detail in the following paper [3].

From the point of view of hyperfine interactions, Fe atoms located in the intermediate region between the bulk of the crystalline Fe grains and the 'pure' amorphous residual phase, i.e. atoms (ii) and (iii), are expected to show similar behaviour. This may well

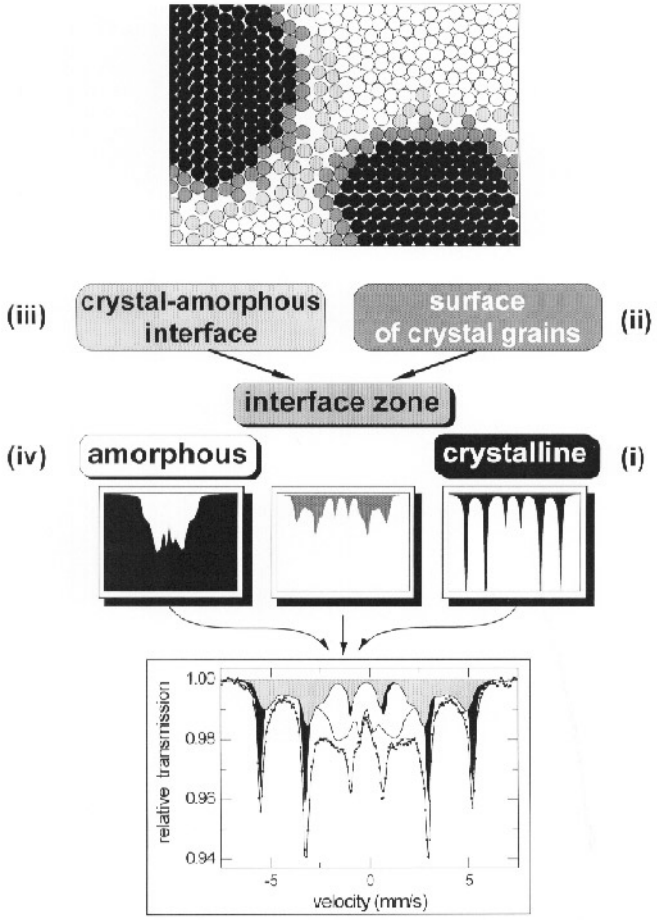

Figure 1. A schematic representation of a nanocrystalline structure and the corresponding Mössbauer spectrum (see the text).

also be why the temperature dependencies of the magnetization decay much more slowly for nanocrystalline alloys than for as-quenched alloys, and, consequently, why the Curie temperature of the amorphous remainder cannot be precisely determined; indeed, a transition region of the magnetic ordering temperature is observed [33].

On the basis of the above discussion, we have introduced a fitting model which consists in general of three main components, as shown in the bottom part of figure 1: one sextet of lorentzian lines and two independent subspectra resulting from the distribution of magnetic sextets. The first one is ascribed to the bulk of α-Fe nanocrystalline-grain atoms (i). One distribution block with low hyperfine fields (up to about 20 T) represents the amorphous-residual-matrix atoms (iv), and can be decomposed eventually into two components: one consisting of Fe atoms in a paramagnetic state corresponding to the prevailing electric quadrupolar interactions; and the second consisting of those in a magnetically ordered state. This situation will be described on the basis of high-temperature Mössbauer spectra (as an example, the case of $Fe_{73.5}Nb_{4.5}Cr_5Cu_1B_{16}$ nanocrystalline alloys is presented below, where the presence of Cr significantly decreases the magnetic ordering temperature of

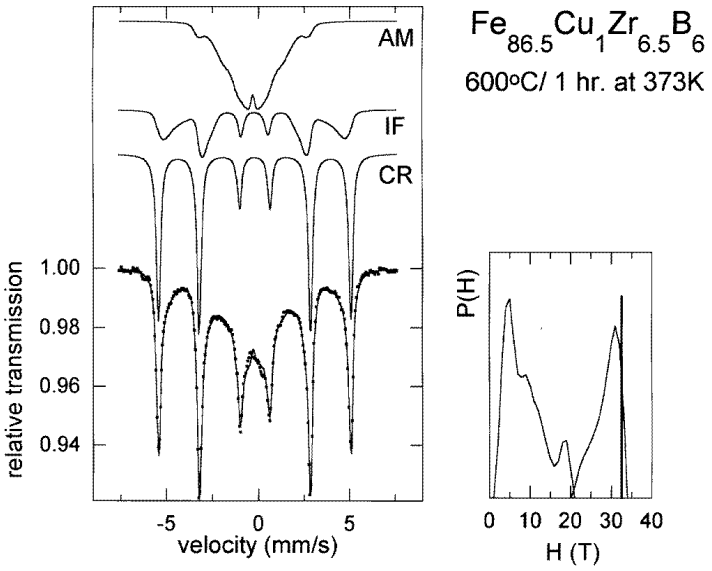

Figure 2. The Mössbauer spectrum of the $Fe_{86.5}Zr_{6.5}Cu_1B_6$ nanocrystalline alloy (600 °C/1 h) recorded at 373 K, with the corresponding $P(H)$ distributions.

the corresponding amorphous remainder). Since Fe atoms (ii) and (iii) are practically indistinguishable from both the structural and the magnetic points of view, in the following we will refer to them as the interface zone. The second distribution block is consequently attributed to this interface zone.

By dividing one single (although double-peaked) $P(H)$ curve [18–22] into two or more components, we are able to account for the different structural and magnetic origins of Fe atoms as introduced by figure 1. It is obvious that the chemical short-range order of Fe atoms located in the amorphous residual matrix varies to a larger extent (due to segregation of α-Fe) than that of the interface atoms. This phenomenon would be manifested by different spectral parameters, e.g. average isomer shifts, independently refined from two distribution blocks. This is not possible to achieve using only a single $P(H)$ model where the particular isomer shift values are coupled with the H-values over the whole H-range with the same constant. Thus, our fitting method is superior to the usual 'model-independent' single-$P(H)$ approach because it provides more realistic spectral parameters of Fe atoms located in chemically and topologically inequivalent positions.

All of the spectral parameters of the lorentzian sextet, i.e. the hyperfine field (H), the isomer shift (δ), the full linewidth (FWHM), and the intensity ratio of the second/fifth to the third/fourth line D23, are fitted. The distribution blocks are composed of individual sextets with the same linewidth, whose value was taken as identical to that of an α-Fe calibration foil (FWHM = 0.28 mm s^{-1}). The hyperfine fields increase stepwise ($\Delta H = 1$ T) from 0 T to about 20 T and from about 20 T to about 35 T for the amorphous-residual-phase (AM) and the interface-zone (IF) components, respectively. It is noteworthy that the ranges of H-values depend on the sample and/or the temperature of the measurement; they have to be determined according to the procedure which is described below. The isomer shift of the ith discrete sextet is calculated as $IS_i = IS_0 + i\,DTI$ and is related to the respective hyperfine-field value. The isomer shift of the first sextet IS_0 as well as the linear coefficient DTI are

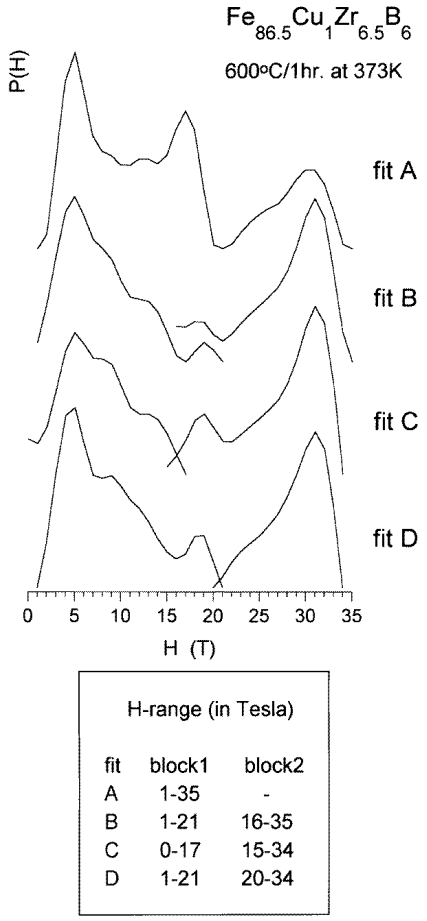

Figure 3. $P(H)$ distributions corresponding to the $Fe_{86.5}Zr_{6.5}Cu_1B_6$ nanocrystalline alloy (600 °C/1 h) at 373 K obtained by different fitting procedures (see the text).

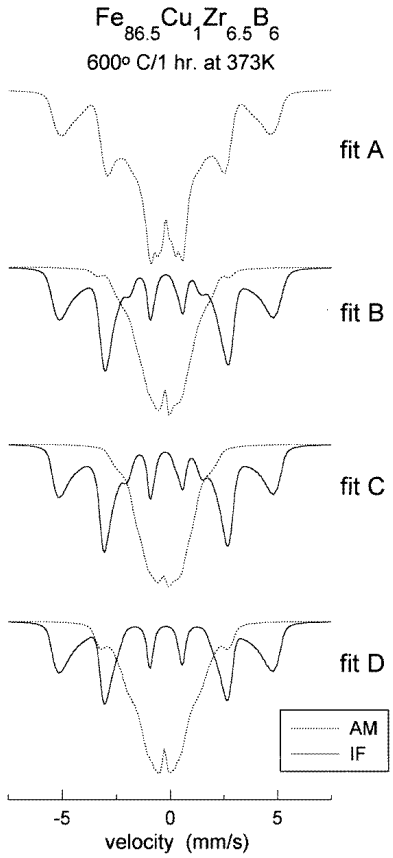

Figure 4. Components of the theoretical Mössbauer spectra corresponding to the different $P(H)$ distributions of figure 3.

fitted for the two distribution blocks separately. The mean values δ of the isomer shift for the AM and IF components are expressed as $\delta = \sum(\mathrm{IS}_i P(H_i))/\sum P(H_i)$. The relative intensity ratios D23 of the individual sextets are assumed to be the same for all components within each distribution block, and are also refined for both components separately. For the sake of simplicity, the quadrupolar shifts of both the crystalline sextet and the individual components of the two distributions are constrained to be zero.

5. Application of the present fitting model to FeMCuB nanocrystalline alloys

5.1. $Fe_{86.5}Zr_{6.5}Cu_1B_6$ nanocrystalline alloys

Figure 2 illustrates an example of the fitting procedure described above applied to an $Fe_{86.5}Zr_{6.5}Cu_1B_6$ alloy, which was thermally treated at 600 °C for one hour. Thus, the corresponding Mössbauer spectrum recorded at 373 K consists of three components: two

Table 1. Parameters of $Fe_{86.5}Cu_1Zr_{6.5}B_6$ nanocrystalline (600 °C/1 h) Mössbauer spectrum as derived from the fittings according to different models: the minimum and the maximum values of the $P(H)$ distribution H_{min} and H_{max}, respectively; the mean value of $P(H)$, $\langle H\rangle$; its standard deviation, σ; the full width, Γ; the isomer shift, δ (with respect to the spectrum of bcc-Fe at 300 K); the line intensity ratio, D23; and the relative area of the respective component, A_{rel}. The statistical errors in the last digits are given in brackets. The errors in the determination of H_{eff}, Γ, δ, D23, and A_{rel} are estimated to be ±0.15 T, ±0.03 mm s^{-1}, ±0.03 mm s^{-1}, ±0.15, and ±2%, respectively. The Mössbauer spectrum was recorded at 373 K.

Amorphous residual matrix—AM							
Fit	H_{min} (T)	H_{max} (T)	$\langle H\rangle$ (T)	σ (T)	$\langle\delta\rangle$ (mm s^{-1})	D23	A_{rel} (%)
A	1	35	14.5(4)	9.1(2)	−0.07	0.4	55
B	1	21	7.6(4)	4.0(4)	−0.14	1.6	31
C	0	17	8(2)	4(1)	−0.13	3.0	30
D	0	21	8.8(3)	4.7(2)	−0.13	0.8	36
Interface zone—IF							
Fit	H_{min} (T)	H_{max} (T)	$\langle H\rangle$ (T)	σ (T)	$\langle\delta\rangle$ (mm s^{-1})	D23	A_{rel} (%)
A	—	—	—	—	—	—	—
B	16	35	27.4(6)	4.8(4)	−0.07	3.5	29
C	15	34	27(2)	4(1)	−0.08	3.6	30
D	20	34	28.9(5)	3.0(4)	−0.06	3.3	23
Crystalline phase—CR							
Fit	H_{min} (T)	H_{max} (T)	H_{eff} (T)	Γ (mm s^{-1})	δ (mm s^{-1})	D23	A_{rel} (%)
A	—	—	32.6	0.29	−0.04	3.6	45
B	—	—	32.6	0.27	−0.04	3.2	40
C	—	—	32.6	0.27	−0.04	3.2	40
D	—	—	32.6	0.27	−0.04	3.3	41

distributions of sextets attributed to the AM and to the IF, and a single sextet of lorentzian lines ascribed to α-Fe nanocrystalline grains (CR). The resulting profile is shown in figure 2 by a solid line running through the experimental data (solid dots). Distributions of hyperfine fields $P(H)$ which have been derived from AM- and IF-broadened subspectra are illustrated on the right-hand side of figure 2. The position and height of the thick vertical line represent the hyperfine-field value and the relative area of the CR component, respectively. The $P(H)$ scale of this line is reduced by a factor of ten with respect to the $P(H)$ scale of the two distribution blocks.

The procedure for finding the appropriate limits of the hyperfine-field distributions for the AM and IF components can be explained with the help of four different fits which have been applied to the Mössbauer spectrum recorded at 373 K for the $Fe_{86.5}Zr_{6.5}Cu_1B_6$ alloy annealed at 600 °C for 1 h. Figure 3 illustrates the $P(H)$ distributions derived, and the broadened subspectra attributed to the AM and IF contributions are compared in figure 4. Refined values of all of the spectral parameters are listed in table 1.

The fit labelled A in figure 3 uses a single $P(H)$ distribution block ranging from 1 T to 35 T—an approach which has already been frequently employed [18–22]. Three pronounced peaks positioned at about 5 T, 17 T, and 30 T can be distinguished in the

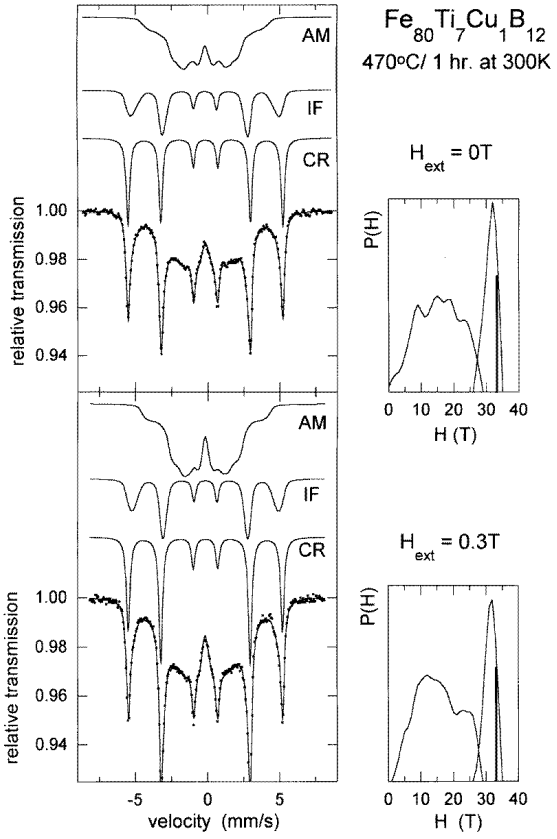

Figure 5. Room temperature Mössbauer spectra of the $Fe_{80}Ti_7Cu_1B_{12}$ nanocrystalline alloy (470 °C/1 h) recorded without and with an external magnetic field. The corresponding $P(H)$ distributions are given on the right-hand side.

uppermost $P(H)$ curve of figure 3. Near-zero $P(H)$ values at around 20 T suggest that two distinct Fe environments exist in the nanocrystalline alloy, and that the resulting $P(H)$ should be divided into two independent blocks. Another argument for splitting the single-block $P(H)$ arises from the line overlap. One should bear in mind that a significant contribution to the intensity of the $P(H)$ peak close to about 17 T corresponds to the positions of the intermediate lines (fifth and second) of the sextets with $H \approx 30$ T, whose intensity is strongly dependent on the ferromagnetic domain texture, i.e. the distribution of the orientations of the magnetic moments.

The fit labelled B results from two overlapped hyperfine-field distributions. As can be seen from figure 3, the $P(H)$ values of the second distribution block (ranging from 16 T to 35 T) are rather large near the lower limit (16 T) and tend to increase further. This is a consequence of the line overlap as outlined above. Consequently, the limits were shifted towards lower H-values, leading to the fit labelled C. The rather large statistical errors obtained (listed in table 1) militate against this latter procedure. Moreover, the double-peak structure of the IF component of $P(H)$ (IF-$P(H)$) is caused by the line overlap and by the deformation of the intermediate lines of the high-field subspectrum, as justified in the previous case (see the solid line in figure 4, fits B and C).

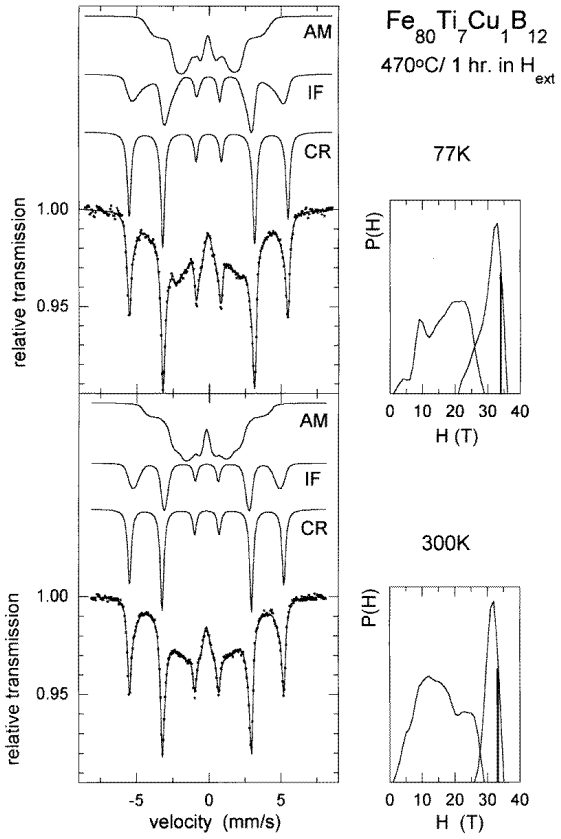

Figure 6. In-field Mössbauer spectra of the $Fe_{80}Ti_7Cu_1B_{12}$ nanocrystalline alloy (470 °C/1 h) taken at 77 K and 300 K. The corresponding $P(H)$ distributions are given on the right-hand side.

The most satisfactory fitting procedure is displayed in figure 2 as fit D (see also figures 3 and 4). The IF component can be assigned to the atoms of the crystalline-grain surface because the position of the main $P(H)$ peak, the isomer shift, and the line intensity ratio D23 (listed in table 1) are all very close to the values obtained for the crystalline component. A tail in IF-$P(H)$ in the vicinity of 23 T is supposed to correspond to atoms (ii) described above. The high-field tail in the AM component of $P(H)$ (AM-$P(H)$) positioned at about 18 T is attributed to atoms (iii) contained in the AM component.

It is noteworthy that the CR component is well defined and exhibits the same values of the hyperfine parameters for fits B, C, and D, regardless of the limits of the $P(H)$ distributions, as is evident from table 1. In fit A, slightly higher values of the FWHM and D23 lead to an increase in the relative area A_{rel}. Such a feature indicates a tendency of the CR contribution to compensate for the lack of an IF component in this one-distribution-block fitting model. The hyperfine parameters of the CR component clearly demonstrate that the crystalline phase is α-Fe [34].

A small overlap is seen in fit D presented in figure 4 between the outermost lines of the AM component and the intermediate lines of the IF one, leading to a miscount of the atom (ii) and atom (iii) contents. To account properly for the overlapping range and to ensure

that it does not stem from the fitting procedure itself, Mössbauer effect measurements were performed in the presence of an external magnetic field. The latter was oriented parallel to the plane of the ribbon, inducing a completely in-plane arrangement of the magnetic moments. Consequently, the fitting procedure could be simplified because one can assume a fixed line intensity ratio of 3:4:1:1:4:3 (D23 = 4).

Table 2. Parameters of the $Fe_{80}Ti_7Cu_1B_{12}$ nanocrystalline (470 °C/1 h) Mössbauer spectrum taken at 300 K without and with an external magnetic field H_{ext}: the minimum and the maximum value of the $P(H)$ distribution H_{min} and H_{max}, respectively; the mean value of $P(H)$, $\langle H\rangle$; its standard deviation, σ; the full width, Γ; the isomer shift, δ (with respect to the spectrum of bcc-Fe at 300 K); the line intensity ratio, D23; and the relative area of the respective component, A_{rel}. The statistical errors in the last digits are given in brackets. The errors in the determination of H_{eff}, Γ, δ, D23, and A_{rel} are estimated to be ±0.15 T, ±0.03 mm s^{-1}, ±0.03 mm s^{-1}, ±0.15, and ±2%, respectively.

Amorphous residual matrix—AM							
H_{ext} (T)	H_{min} (T)	H_{max} (T)	$\langle H\rangle$ (T)	σ (T)	$\langle\delta\rangle$ (mm s^{-1})	D23	A_{rel} (%)
0	0	29	15.4(9)	6.5(6)	−0.01	4	47
0.3	2	25	15.3(7)	6.5(5)	−0.01	4[a]	50
0.05[b]	1	29	16.9(7)	5.9(4)	0.08	4[a]	42
Interface zone—IF							
H_{ext} (T)	H_{min} (T)	H_{max} (T)	$\langle H\rangle$ (T)	σ (T)	$\langle\delta\rangle$ (mm s^{-1})	D23	A_{rel} (%)
0	26	35	31.2(8)	1.8(9)	−0.01	3.8	23
0.3	27	35	31.2(5)	1.7(5)	0.00	4[a]	21
0.05[b]	22	36	30.6(5)	3.1(3)	0.12	4[a]	28
Crystalline phase—CR							
H_{ext} (T)	H_{min} (T)	H_{max} (T)	H_{eff} (T)	Γ (mm s^{-1})	δ (mm s^{-1})	D23	A_{rel} (%)
0	—	—	33.3	0.28	0.00	2.9	30
0.3	—	—	33.3	0.29	0.01	4[a]	29
0.05[b]	—	—	34.1	0.30	0.12	4[a]	30

[a]Fixed during fitting.
[b]The temperature of the measurement $T = 77$ K.

5.2. $Fe_{80}Ti_7Cu_1B_{12}$ nanocrystalline alloys

We illustrate the applicability of the present fitting procedure, including the effect of an external magnetic field, for an $Fe_{80}Ti_7Cu_1B_{12}$ nanocrystalline alloy. The thermal treatment at 470 °C for 1 h leads to the occurrence of α-Fe nanocrystalline grains, as confirmed by x-ray diffraction measurements [24]. Mössbauer spectra recorded at 300 K without and with an external magnetic field are presented in figure 5, while others taken at 77 K and 300 K in an external field are shown in figure 6. Individual subspectra and the corresponding distributions of hyperfine fields are also displayed. The values of the spectral parameters are listed in table 2. Only an illustration for the present purpose is presented below; detailed results concerning $Fe_{80}Ti_7Cu_1B_{12}$ nanocrystalline alloys will be reported in a forthcoming paper.

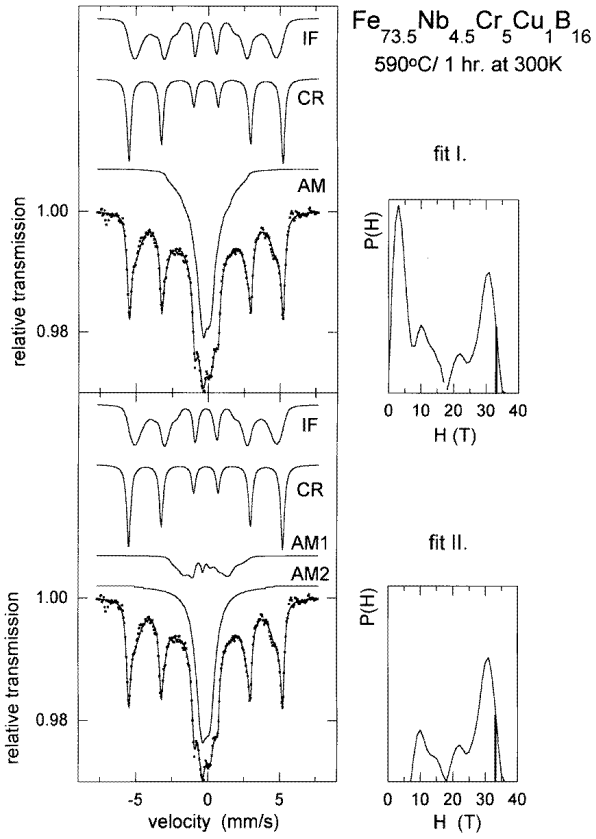

Figure 7. Room temperature Mössbauer spectra of the $Fe_{73.5}Nb_{4.5}Cr_5Cu_1B_{16}$ nanocrystalline alloy (590 °C/1 h), and the corresponding $P(H)$ distributions, as obtained from different fitting models (see the text).

The parameter D23 was constrained to be D23 = 4 for the in-field spectra. The other parameters are the same as at room temperature within the experimental errors. As shown in figure 5, differences between the 300 K Mössbauer spectra taken without and with an external magnetic field proceed from the shape of the $P(H)$ distributions in the AM component only (apart from line intensities). No appreciable changes in the shape and/or parameters of the $P(H)$ block attributed to the IF component are observed.

The in-field Mössbauer spectra taken at different temperatures and presented in figure 6 exhibit some modifications due to changes in the character of the magnetic ordering within the AM as well as the IF components. As a consequence, magnetic hyperfine fields with higher H-values are more pronounced at low temperature.

5.3. $Fe_{73.5}Nb_{4.5}Cr_5Cu_1B_{16}$ nanocrystalline alloys

Let us examine fit D of the Mössbauer spectrum of the $Fe_{86.5}Zr_{6.5}Cu_1B_6$ nanocrystalline alloy presented in figure 4: the subspectrum due to the AM component exhibits broad lines and a complex hyperfine structure originating from the simultaneous presence of both quadrupolar electric and dipolar magnetic interactions, especially at elevated temperatures.

It has been frequently observed that the hyperfine structure of FeZr amorphous alloys is strongly dependent on the Zr content [35, 36]. This suggests a heterogeneous content of Fe and Zr within the AM phase in the case of $Fe_{86.5}Zr_{6.5}Cu_1B_6$ nanocrystalline alloys, due to the presence of Zr. Consequently, the best fitting procedure for the subspectrum due to the AM component would introduce a decomposition of the distribution block into two parts, but this complex spectral situation prevents a simple treatment. That is why we were interested in $Fe_{73.5}Nb_{4.5}Cr_5Cu_1B_{16}$ nanocrystalline alloys (annealed at 590 °C for 1 h)—the situation is less complex from the point of view of hyperfine interactions.

Table 3. Parameters of the $Fe_{73.5}Nb_4Cr_5Cu_1B_{16}$ nanocrystalline (590 °C/1 h) room temperature Mössbauer spectrum as derived from fittings to different models: the minimum and the maximum value of the $P(H)$ distribution H_{min} and H_{max}, respectively; the mean value of $P(H)$; $\langle H\rangle$; its standard deviation, σ; the full width, Γ; the isomer shift, δ (with respect to the spectrum of bcc-Fe at 300 K); the line intensity ration, D23; and the relative area of the respective component, A_{rel}. The statistical errors in the last digits are given in brackets. The errors in the determination of H_{eff}, Γ, δ, D23, and A_{rel} are estimated to be ±0.15 T, ±0.03 mm s^{-1}, ±0.03 mm s^{-1}, ±0.15, and ±2%, respectively.

Amorphous residual matrix—AM							
Fit	H_{min} (T)	H_{max} (T)	$\langle H\rangle$ (T)	σ (T)	$\langle\delta\rangle$ (mm s^{-1})	D23	A_{rel} (%)
I	0	18	6.3(1)	4.5(1)	−0.02	2.2	47
II	7	18	11.5(4)	2.5(4)	0.07	2.3	10
II	—	—	0.60(1)[a]	0.9[b]	−0.01	0.87[c]	38
Interface zone—IF							
Fit	H_{min} (T)	H_{max} (T)	$\langle H\rangle$ (T)	σ (T)	$\langle\delta\rangle$ (mm s^{-1})	D23	A_{rel} (%)
I	18	36	28.3(5)	4.0(4)	−0.02	1.9	31
II	18	36	28.6(8)	3.9(3)	−0.01	2	31
Crystalline phase—CR							
Fit	H_{min} (T)	H_{max} (T)	H_{eff} (T)	Γ (mm s^{-1})	δ (mm s^{-1})	D23	A_{rel} (%)
I	—	—	33.2	0.31	0.00	2.3	22
II	—	—	33.2	0.31	0.00	2.2	21

[a]Quadrupole splitting of the doublet in mm s^{-1}.
[b]FWHM of the doublet in mm s^{-1} (≈2.8 T).
[c]The line intensity of the doublet, D21.

Its room temperature Mössbauer spectrum was first analysed using the present fitting procedure as discussed in section 4. The results of fit I are presented in the upper part of figure 7 and in table 3. A pronounced peak in $P(H)$ corresponding to the AM phase is localized at about 3 T. It indicates a collapse of the ferromagnetic exchange interactions in a certain portion of the amorphous residual phase and should be ascribed to the prevailing quadrupolar electric interactions. Such an experimental feature reinforces the hypothesis of a heterogeneous chemical character of the amorphous matrix. For that reason, we have adopted another procedure (fit II) which consisted in replacing the low magnetic fields of AM-$P(H)$ by a quadrupolar component. In other words, we have decomposed the original subspectrum due to the AM phase into two components, AM1 and AM2, which are restored using a distribution of magnetic sextets and an asymmetrical quadrupolar doublet

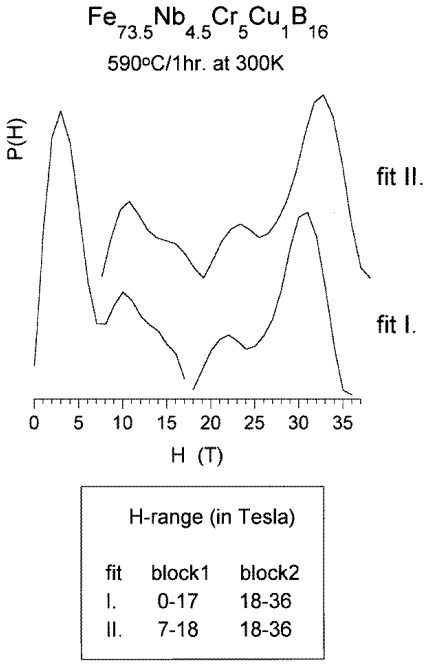

Figure 8. $P(H)$ distributions corresponding to the 300 K Mössbauer spectrum of the $Fe_{73.5}Nb_{4.5}Cr_5Cu_1B_{16}$ nanocrystalline alloy (590 °C/1 h) obtained from different fitting models (see the text).

with broad lorentzian lines, respectively. First, we used the 1989 version of the NORMOS DIST program which allows treatment of only two distribution blocks of the same nature (magnetic fields or quadrupolar splittings). That is why the distribution of quadrupolar splittings in fit II was modelled by a broadened doublet of lorentzian lines; the ratio of the line intensities of the doublet, D21, was free during the fitting procedure, to account for its asymmetry. The results obtained were very close to those obtained by means of the MOSFIT program which allows the use of independent distributions of both the hyperfine field and the quadrupolar splitting, and single components; the doublet was generated with correlated distributions of the isomer shift and the quadrupolar splitting to account for the asymmetry. The Mössbauer spectrum with all of these components, as well as the hyperfine fields corresponding to the AM1, IF, and CR phases, are illustrated in the bottom part of figure 7; the refined values of the hyperfine parameters are collected together in table 3.

Figure 8 provides a detailed picture of the $P(H)$ distributions for fits I and II. Their shapes are very similar in the range 7 T to 18 T, corresponding to the AM phase. Only slight modifications can be seen, at around 17 T, due to the line overlap in fit I which is less favourable, because of the magnetic texture effects.

6. Conclusions

A novel approach has been proposed for fitting Mössbauer spectra of Fe(Cu)MB-type nanocrystalline alloys. The fitting model consists of three main components in agreement with the expected atomic representation of a nanocrystalline alloy:

(a) a single sextet of lorentzian lines attributed to the bulk of α-Fe nanocrystalline grains;

(b) a distribution of sextets ascribed to resonant Fe atoms located in the amorphous residual matrix; and

(c) a distribution of sextets of the so-called interface zone which comprises Fe atoms situated in the crystal grains' surface as well as those in the nanocrystal-to-amorphous interface, originating from the amorphous precursor and in close contact with the nanocrystalline grains.

The component (b) might be eventually decomposed into two parts, accounting for the presence of simultaneous electric and magnetic hyperfine interactions: this suggests an extremely heterogeneous composition of the amorphous residual matrix, resulting from the diffusion mechanisms associated with the nanocrystallization process.

The results of the fittings enable us to estimate the effective thickness t of the interface zone. If we assume that the crystalline grains are spherical in shape with a diameter d, the ratio $(A(\mathrm{IF}) + A(\mathrm{CR}))/A(\mathrm{CR}) \approx (1 + 2t/d)^3$. Considering equal f-factors for each structural position of Fe atoms within the samples studied, we obtain from (i) table 1, rows D, (ii) table 2, the average over all rows, and (iii) table 3, rows II, that $t/d \approx 0.08$, 0.11, and 0.18, respectively. Taking into account that the average grain diameter is about 10–20 nm, the estimated interface-zone thickness would be about 1–4 nm.

The fitting procedure proposed in this paper is applied to Fe-based nanocrystalline alloys which do not contain Si atoms. This is a crucial point since the crystalline phase that emerges during the first stage of crystallization is α-Fe, leading to only one sextet whose hyperfine parameters are well known. In principle, this fitting procedure could be applied for nanocrystalline alloys which exhibit more crystalline phases, or one crystalline phase with different iron sites. Such a situation is encountered in systems containing Si, but in the latter case, the too-complex hyperfine structure prevents one from finding an accurate and precise interpretation, because one will be faced with the problem of overlapping lines. Nevertheless, we demonstrate in the present study that the problem of line overlap could be satisfactorily dealt with by performing in-field Mössbauer experiments: the knowledge of the orientation of the magnetization allows one to eliminate ambiguities stemming from unknown line intensities. The magic-angle configuration may *a priori* lead to some simplifications, but one has to check the free-texture behaviour for the different components [37].

The novel fitting model introduced here opens up new areas in the investigation of nanocrystalline materials via the study of hyperfine interactions of atoms in different structural positions, in conjunction with the intrinsic character of the material. Detailed analysis of the corresponding $P(H)$ distributions, aided by a 3-D mapping of the hyperfine-field distribution combined with a third instrumental parameter (the measurement temperature, annealing temperature, external field, ...) enables a topography of hyperfine fields to be obtained. Part II of this article (the following paper) concerns the application of the present fitting method to establish the topography of hyperfine interactions in $Fe_{87.5-x}Cu_xZr_{6.5}B_6$ $(x = 0, 1)$ nanocrystalline alloys.

Acknowledgments

Fruitful discussions with Dr I Škorvánek (Košice) and Dr A Ślawska-Waniewska (Warsaw) in the early stages of this work are gratefully acknowledged. Ribbons of the $Fe_{86.5}Zr_{6.5}Cu_1B_6$ and $Fe_{73.5}Nb_{4.5}Cr_5Cu_1B_{16}$ amorphous alloys were provided by courtesy of Dr P Duhaj and

Dr P Švec (Bratislava). The $Fe_{80}Ti_7Cu_1B_{12}$ nanocrystalline alloys were prepared by Dr B Idzikowski (Poznan) in the framework of the the EC project CIPA CT 94-0208. MM is indebted to the Région Pays de la Loire for financial support during his stay at Le Mans.

References

[1] Herzer G 1989 *IEEE Trans. Magn.* **25** 3327
Herzer G 1990 *IEEE Trans. Magn.* **26** 1397
[2] Campbell S J and Gleiter H 1993 *Mössbauer Spectroscopy Applied to Magnetism and Material Science* vol 1, ed G J Long and F Grandjean (New York: Plenum) pp 241–304
[3] Miglierini M and Greneche J M 1997 *J. Phys.: Condens Matter* **9** 2321–47
[4] Gonser U and Preston R 1983 *Topics in Applied Physics: Glassy Metals (II)* ed H Beck and H J Guntherodt (Berlin: Springer) pp 93–126
[5] Longworth G 1987 *Mössbauer Spectroscopy Applied to Inorganic Chemistry* vol 2, ed G J Long (New York: Plenum) pp 289–342
[6] Le Caër G, Dubois J M, Fischer H, Gonser U and Wagner H G 1984 *Nucl. Instrum. Methods* B **5** 25–33
[7] Greneche J M and Varret F 1982 *J. Phys. C: Solid State Phys.* **15** 5333–44
[8] Campbell S J and Aubertin F 1987 *Mössbauer Spectroscopy Applied to Inorganic Chemistry* vol 3, ed G J Long and F Grandjean (New York: Plenum) pp 183–242
[9] Jiang J, Aubertin F, Gonser U and Hilzinger H R 1991 *Z. Metallk.* **82** 698–702
[10] Hampel G, Pundt A and Hesse J 1992 *J. Phys.: Condens. Matter* **4** 3195–214
[11] Rixecker G, Schaaf P and Gonser U 1992 *J. Phys.: Condens. Matter* **4** 10 295–310
[12] Gupta A, Bhagat N and Principi G 1995 *J. Phys.: Condens. Matter* **7** 2237–48
[13] Pundt A, Hampel G and Hesse J 1992 *Z. Phys.* B **87** 65–72
[14] Zatroch M, Petrovič P and Brovko I 1992 *Nucl. Instrum. Methods* **72** 462–6
[15] Zemčík T 1993 *Key Eng. Mater.* **81–83** 261–6
[16] Miglierini M 1994 *J. Phys.: Condens. Matter* **6** 1431–8
[17] Pradell T, Clavaguera N, Zhu J and Clavaguera-Mora M T 1995 *J. Phys.: Condens. Matter* **7** 4129–43
[18] Miglierini M 1996 *Hyperfine Interact.* C **1** 254–7
[19] Gorría P, Orúe I, Plazaola F, Fernández-Gubieda M L and Barandiarán J M 1993 *IEEE Trans. Magn.* **29** 2682–4
[20] Orúe I, Gorría P, Plazaola F, Fernández-Gubieda M L and Barandiarán J M 1994 *Hyperfine Interact.* **94** 2199–205
[21] Navarro I, Hernando A, Vázquez M and Yu Seong-Cho 1995 *J. Magn. Magn. Mater.* **145** 313–8
[22] Gómez-Polo C, Holzer D, Multinger M., Navarro I, Agudo P, Hernando A, Vázquez M, Sassik H and Grössinger R 1996 *Phys. Rev.* B **53** 3392–7
[23] Miglierini M, Labaye Y, Randrianantoandro N and Greneche J M 1997 *Mater. Sci. Eng.* at press
[24] Miglierini M and Greneche J M 1997 *J. Czech. Phys.* at press
[25] Randrianantoandro N, Greneche J M, Jędryka E, Ślawska-Waniewska A and Lachowicz H K 1995 *Mater. Sci. Forum* **179–181** 545–50
[26] Randrianantoandro N, Ślawska-Waniewska A and Greneche J M 1997 *Phys. Rev.* B submitted
[27] Duhaj P, Mat'ko I, Švec P, Sitek J and Janičkovič D 1996 *Mater. Sci. Eng.* B **39** 208–15
[28] Ślawska-Waniewska A, Zuberek R and Nowicki P 1996 *J. Magn. Magn. Mater.* **157+158** 147–8
[29] Brand R A 1989 *NORMOS program* 1989 version, unpublished
[30] Teillet J and Varret F *MOSFIT program* unpublished
[31] Hernando A and Kulik T 1994 *Phys. Rev.* B **49** 7064–7
[32] Navarro I, Ortuño M and Hernando A 1996 *Phys. Rev.* B **53** 11 656–60
[33] Ślawska-Waniewska A and Nowicki P 1995 *Mater. Sci. Forum* **179–181** 563–8
[34] Preston R S, Hanna S S and Heberle J 1962 *Phys. Rev.* **128** 2207–18
[35] Nasu S, Miglierini M, Kitagawa H and Fukamichi K 1994 *Hyperfine Interact.* **84** 177–81 and references therein
[36] Ryan D H, Coey J M D, Batalla E, Altounian Z and Ström-Olsen J O 1987 *Phys. Rev.* B **35** 8630–8
[37] Greneche J M and Varret F 1982 *J. Physique Lett.* **43** L233–7